## CONFERENCE PRE-PRINT

## ICRH SYSTEM FOR THE HL-3 TOKAMAK

Ling-Feng Lu, Jun Liang, Ya-Li Chen, Cheng-Gong-Hang Zhou, Chu-Rui Zhang, Zhi Li, Yue-Xin Ma, Xing-Yu Bai

Southwestern Institute of Physics Chengdu, People's Republic of China Email: lulingfeng@swip.ac.cn

Bo Lu ITER organization Saint Paul Les Durance Cedex

## **Abstract**

The HL-3 tokamak is a new medium-sized copper conductor tokamak at Southwestern Institute of Physics (SWIP). In order to provide central ion heating as well as generate energetic particles whose energy level is equivalent to the fusion born alpha particles. 6 MW ion cyclotron range of frequencies (ICRF) power is under construction at SWIP and it will be available in HL-3 at Sep. 2026. Radio Frequency (RF) range 25–50MHz with pulses up to 5s is considered. For a Deuterium plasma, the hydrogen minority and the  $2^{nd}$  harmonic of Deuterium are the main ion heating schemes with f=33MHz at  $B_0$ =2.2T. For a Deuterium-Tritium plasma, the fundamental He-3 and the  $2^{nd}$  harmonic of Tritium with f=25MHz at  $B_0$ =2.5T are considered. The RF generator consists of  $4 \times 1.5$ MW transmitters. The transmission line incorporates 3dB hybrid couplers so as to divert the reflected power. The matching unit is provided by a  $1/4\lambda$  stub tuner and a  $1/2\lambda$  phase shifter, with an additional prematching stub for each of the four transmission lines. Two 2-strap antennas with parallel wavenumber  $k_{II} \sim 6.5$  m<sup>-1</sup> are designed since the impurity issue is supposed to be moderate under a carbon wall.

### 1. INTRODUCTION OF THE HL-3 TOKAMAK

HL-3 is a new medium-sized copper conductor, carbon wall tokamak, previously known as HL-2M [1]. It was built in 2020 at Southwestern Institute of Physics, located in Chengdu, China. Its typical pulse length is about 5s. Since 2020, it has achieved several milestones, such as 1MA plasma current in 2022, 1MA H mode in 2023, 1.5MA H mode in 2024, 13.8keV electron temperature and 10keV ion temperature in 2025 [2].

At present, the total auxiliary heating power in HL-3 is 19.5MW (source power), as shown in Table 1. It will be soon upgraded to 41MW at September 2026 and get ready for the preliminary Deuterium-Tritium operation in 2027. The key roles of ICRF in HL-3 are to provide central ion heating, generate energetic particles that is relevant to the alpha particle physics and maximize the fusion output power in the Deuterium-Tritium campaign around 2030.

	19.5MW before 09/2026	41MW after 09/2026
NBI	12MW, 2 beams, 5MW+7MW	20MW, 3 beams 6MW+7MW+7MW
ECRH	5MW 105GHz+0.5MW 68GHz	4MW 140(175) GHz+2MW 140G+5MW 105GHz
LHCD	2MW 3.7GHz	4MW 3.7GHz
ICRH	0	6MW, 25-50MHz

Table 1. Auxiliary heating power in HL-3

# 2. ICRF HEATING SCHEMES IN HL-3

It is well known that the performance of ICRF heating is better when the Single Pass Absorption (SPA) is high and the cyclotron resonant layer is on axis. FIG 1 depicts the locations of the resonant layer w.r.t. the RF frequency. The major and minor radius of HL-3 are 1.78m and 0.65m, respectively. Accordingly, within the frequency range of 25-50MHz, the main ion heating schemes in a Deuterium plasma are the Hydrogen minority and the  $2^{nd}$  harmonic of Deuterium with f=33MHz at  $B_0$ =2.2T. The overall single pass absorption (Hydrogen minority +  $2^{nd}$  harmonic Deuterium) for a D(H) plasma is above 90% with a typical minority concentration of X[H]=5% and ion temperature of  $T_r$ ~10keV [3]. In the Deuterium-Tritium plasma, the  $2^{nd}$  harmonic of Tritium and the He-3 minority are the main ion heating schemes with f=25MHz at  $B_0$ =2.5T as shown in FIG 2. The overall single pass absorption

(He-3 minority +  $2^{\text{nd}}$  harmonic Tritium) is above 80% with a typical minority concentration of X[He-3]=2% and  $T_i$ ~10keV, as it can be seen in FIG 2 under X[T]=50%, central ion temperature  $T_{i,0}$ =10keV, central electron temperature  $T_{e,0}$ =10keV, central plasma density  $n_{e,0}$ =1.1 ×  $10^{20}$ m<sup>-3</sup>,  $k_{\text{l}}$ =6.5 m<sup>-1</sup>. FIG 3 shows the dependence of the overall SPA in Deuterium-Tritium plasmas on the parallel wavenumber  $k_{\text{l}}$ . A compromise is made in choosing  $k_{\text{l}}$ ~6.5 m<sup>-1</sup>, to ease the power coupling at edge on one hand while maintaining a relatively good power absorption at core on the other hand, *i.e.*, SPA>0.6. Provided the size of the vacuum vessel port in HL-3 is rather small, *i.e.*, 450mm\*500mm, an antenna with  $k_{\text{l}}$ ~6.5 m<sup>-1</sup> has to be installed inside the vacuum vessel. For the purpose of generating energetic ions, simulation shows both the three-ion scheme and synergetic heating with NBI ions are efficient to accelerate ions up to MeV level under typical HL-3 parameters [3].

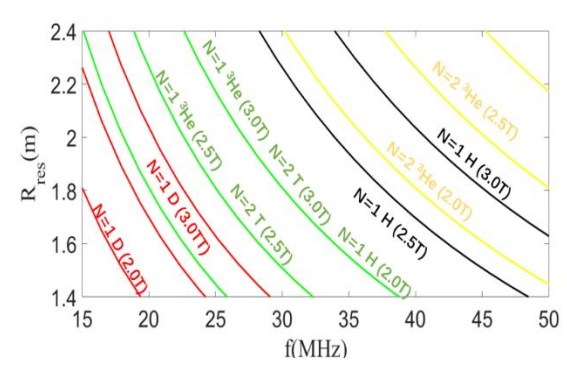
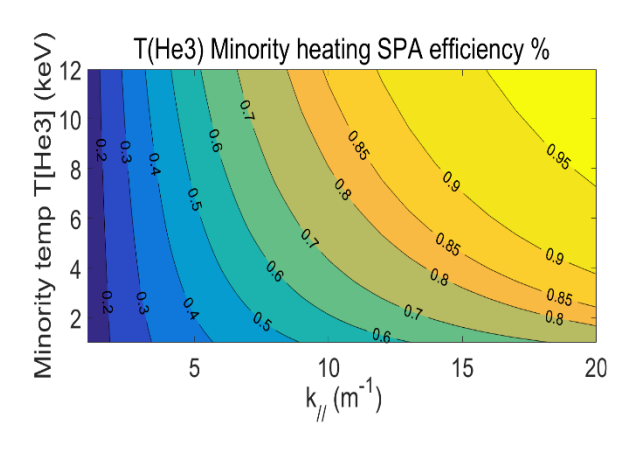


FIG 1. Locations of the cyclotron resonances Vs RF frequency for varies ion species under different B<sub>0</sub>.

FIG 2. Overall Single Pass Absorption (SPA) efficiency (He-3 minority +2<sup>nd</sup> harmonic of T) for a D-T-He-3 plasma Vs minority concentration and ion temperature.

### 3. RF SOURCE AND TRANSMISSION LINE

The RF source consists of a RF actuator and four 1.5MW RF transmitters. Fig. 4 shows the layout of the RF source. The amplitude and phase of the RF actuator are feedback controlled according to the phase and power detectors from the Voltage Current (VI) probe located at the antenna side. Each RF transmitter contains three-stage amplifiers, 6kW solid stage amplifier, 100kW tetrode amplifier and 1.5MW tetrode amplifier. The tetrode amplifiers used for the intermediate stage and final stage are the DB968 from XuGuang company located in Chengdu, China and TH526B from the Thales group in France, respectively.



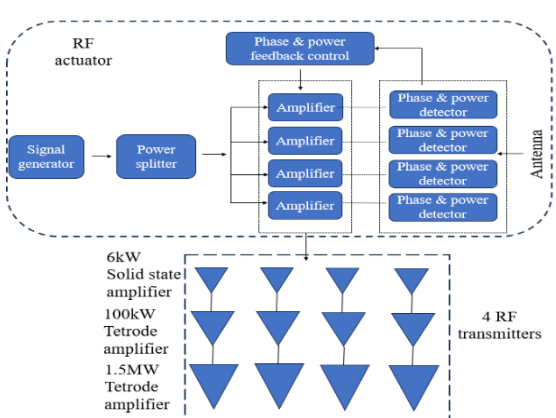


FIG 3. Overall SPA efficiency Vs k// and ion temperature, X[D]=46%, X[He-3]=2%, other conditions are the same as in Fig. 2.

FIG 4. Layout of the RF source for ICRH system in HL-3.

Fig. 5 shows the schematic view of the 6MW ICRF system in HL-3. G1-G4 represent for RF sources as illustrated in Fig. 4. The transmission lines consist of in total 520m coaxial lines and service components. For simplicity, the branches for dummy load test have been neglected in Fig. 5. Two pairs of 3dB hybrid coupler are used to divert the reflection power at the 4 transmission lines to two 50ohm, 500kW dummy loads. By adopting the 3dB hybrid coupler, the four transmitters are bounded together. The whole system will get stuck if any of the four transmitters fails. To prevent this, a branch that skips the 3dB combiner is also added, which was not shown here. In order to

guarantee a  $\pi/2$  phase difference between the two reflected power signals connected to the 3dB decoupler, two phase shifters are added in two of the four transmission lines. The transmission lines are filled with 2bar Nitrogen gas. The matching unit is composed by a phase shifter and a single stub tuner. Calculation shows that with a maximum tuneable length of lambda/2 for the phase shifter and lambda/4 for the stub tuner are enough to cover all the load impedances of our interest, see the green region in FIG 6. In the calculation, the transmission line is categorized as matched if the voltage reflection coefficient at the  $\lambda/4$  stub tuner is less than 1%. In order to further increase the local input impedance, another lambda/8 pre-matching stub is also added after the T connector. The distance between the T connector and the pre-matching stub and the length of the pre-matching stub are optimized to have a minimum reflection coefficient at the T point. For example, FIG 7 shows the voltage reflection coefficient can be at minimum when the distance between the pre-matching stub and T junction is  $0.18\lambda$ , provided the length of the pre-matching stub is  $0.1\lambda$ . An antenna decoupler is also set for each antenna to diminish the interference between the two toroidal straps of the same antenna.

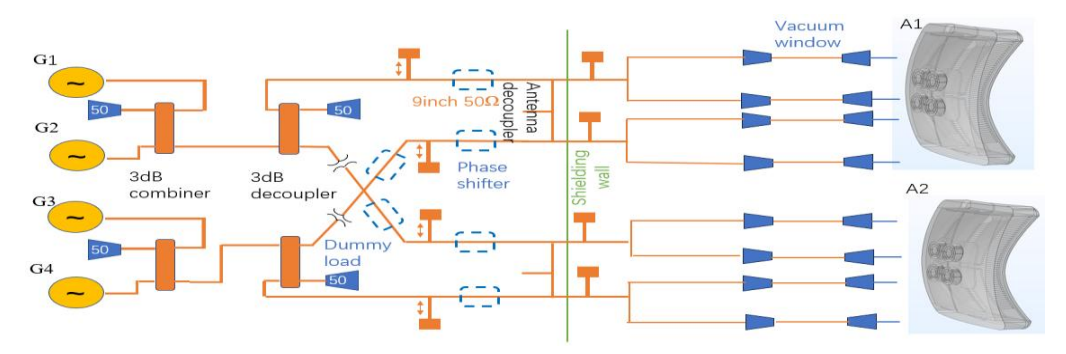


FIG 5. Sketch of the 6MW ICRF system for HL-3.

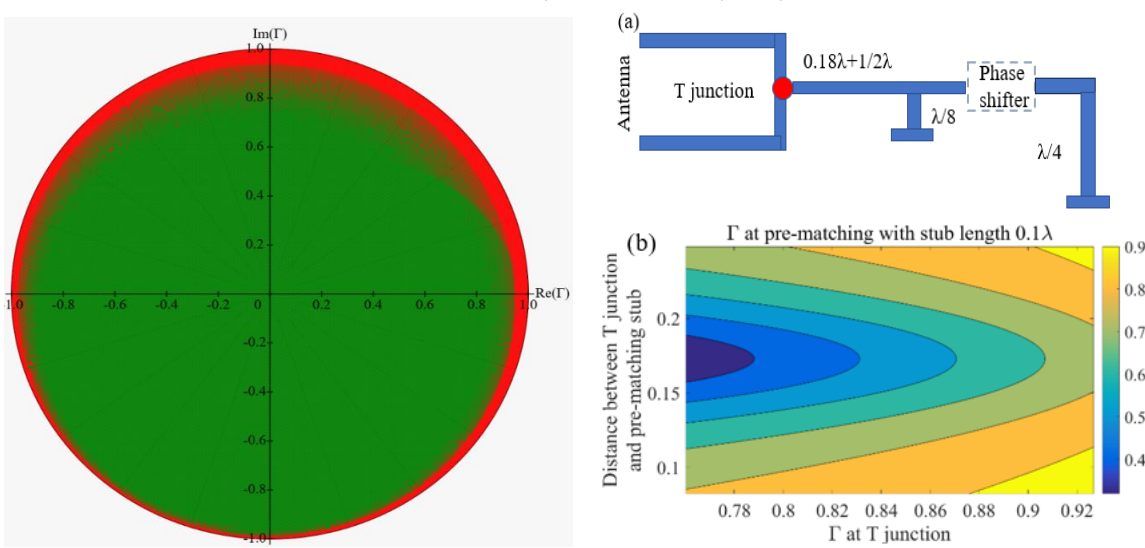


FIG 6. Expected impedance matching performance. Green colour shows the matched region displayed in the Smith chart. RF frequency=33MHz, matched criterion: reflection coefficient at stub tuner <1%.

FIG 7. (a) Matching unit setup in one of the four HL-3 ICRH transmission lines; (b) Variation of the voltage reflection coefficient (Γ) at the location of pre-matching stub w.r.t the Γ value at the T junction, i.e., the red point in (a).

Each of the 4 transmission lines will be split into 2 feed lines via a T connector which then connected to the antenna strap. For the safety reason, each feed line has double vacuum windows [4]. The location of the vacuum windows is put as closest as possible to the antenna straps, while avoiding the locations where the RF voltage or RF current reach the maximum. The T connector and the antenna decoupler are intentionally being put near the voltage maximum points for the adopted two frequencies, *i.e.*, 25MHz and 33MHz as shown in FIG 8, since this set-up has a subsidiary benefit to increase the local input impedance [5]. In FIG 8, the variation of the norm of the electric field along the transmission line is calculated by COMSOL simulations for two most commonly used ICRF frequencies in HL-3, 25MHz & 33MHz. The COMSOL model is a combination of the 3D full wave coupling code developed in [6] and a part of the transmission lines. All the transmission lines are 9 inch 50ohm, except the short parts directly attached to the antenna straps, where a transition from 9 inch to 6 inch is adopted in order to fit through the vacuum vessel port, *i.e.*, the blue segments in FIG 5. At this moment, all the ceramic

window has an outer diameter of 9 inch. Another 6 inch ceramic window is under development. With a 6 inch ceramic window, the distance between the first ceramic window and strap, which is 2m long now, can be further reduced. This may be very helpful in the experiment since this part of transmission line often causes problems. The length difference between the two feed lines coming out from the same T connector is maintained at  $\lambda/2$  which guarantees a poloidal phase difference of  $\pi$  for two adjacent poloidal straps. Some U- bend structures are used to facilitate the length modification if the frequency is shifted from one to another. The antenna toroidal phasing is controlled by adjusting the phasing at the RF actuator. Multiple VI probes and directional couplers are embedded into the coaxial lines to measure the local RF parameters including the VSWR, reflection coefficient and phasing. These signals are then being used in safety protection as well as providing input to the matching algorithm. Some optical fibres are also inserted to detect arcing inside the transmission lines.

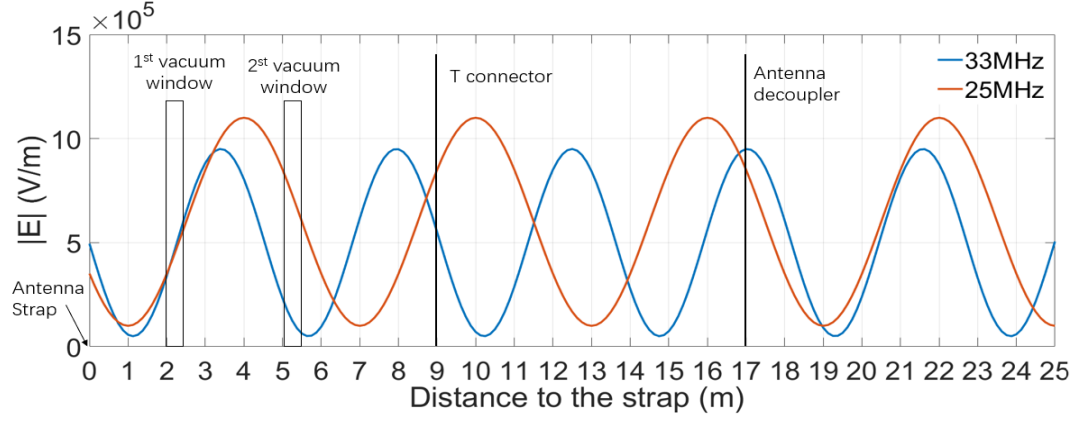


FIG 8. Locations of the vacuum windows, T connector and the antenna decoupler.

### 4. ANTENNA DESIGN

It is decided in the beginning that rather than having an antenna with  $k_0 \sim 13 \text{m}^{-1}$  in order to make the antenna retractable through HL-3 vacuum vessel port, an antenna with larger size but should be installed inside the vacuum vessel is preferred. After taking into consideration of the available size inside the HL-3 vacuum vessel, the finalized antenna size is about 1.2m (toroidally)  $\times$  1.4m (poloidally).

# 4.1 Preliminary electrical analysis

A 2 toroidal strap antenna is chosen since the impurity issue is not expected as serious in a carbon wall machine, like HL-3. No power tapering as having been used intensively in AUG three strap antenna [7] and C-Mod four strap antenna [8] is needed to minimize the RF current on the antenna box. Three types of antenna configurations are considered, which have different feeder connections and ground positions. The antenna configuration which has a larger coupling resistance while maintaining a lower voltage maximum at the feeder is preferred. The electrical circuit models of these three configurations are shown in FIG 9, where  $L_A$  is the electrical length of the strap,  $\lambda_0$  the vacuum wave length,  $Z_L$  the antenna load impedance,  $Z_0$  the character impedance of the antenna,  $Z_T$  the character impedance of the transmission line,  $V_{max}$  the maximum voltage at the transmission line,  $P_{in}$  the input RF power and  $Z_{in}$  the antenna input impedance. A quick analysis based on the electrical circuit model suggests that compared to the antenna configurations with 2 feeder lines, either with central grounded or end grounded, the antenna fed by four feeder lines with end grounded has the minimum  $V_{max}$  at the feeder, as it is shown in FIG 10.

## 4.2 Mechanical constraints

A 2 poloidal by 2 toroidal strap antenna, like the antenna configuration (c) in FIG 9, is thus chosen for further optimization. Since the ICRF system is only designed 4 years after the machine was built, it immediately faces some space constraints inside the vacuum vessel. Firstly, HL-3 is a tokamak designed for high plasma current (Ip) operation, with a maximum Ip=3MA. Thus, a large plasma volume is desired by the operation team. A large plasma size is also favored to obtain a high fusion output power. It is then decided that the antenna could not exceed the first wall at the middle plane. The locations of the first wall in a R-Z (radial-vertical) plane are shown by the yellow curve in FIG 11. This constrains the space available for the antenna installation at the front. Secondly, there are some components that are already present at the potential antenna locations, in particular, the

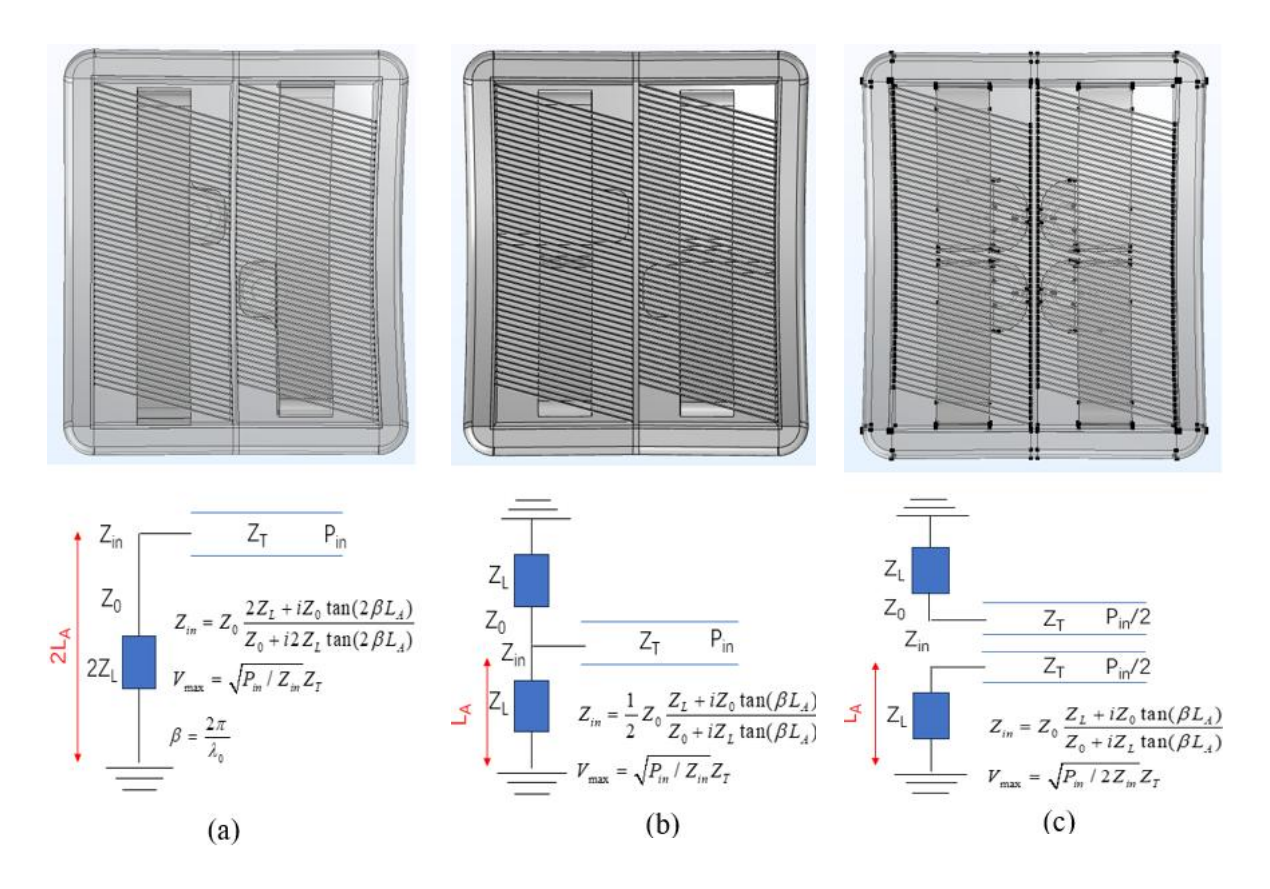


FIG 9. Three types of antenna configurations and their corresponding electrical circuit models. (a) Double feeder lines, each strap forms a single loop, grounded at two poloidal ends; (b) Double feeder lines, each strap forms double loops, grounded at center; (c) Four feeder lines, each strap forms double loops, grounded at two poloidal ends.

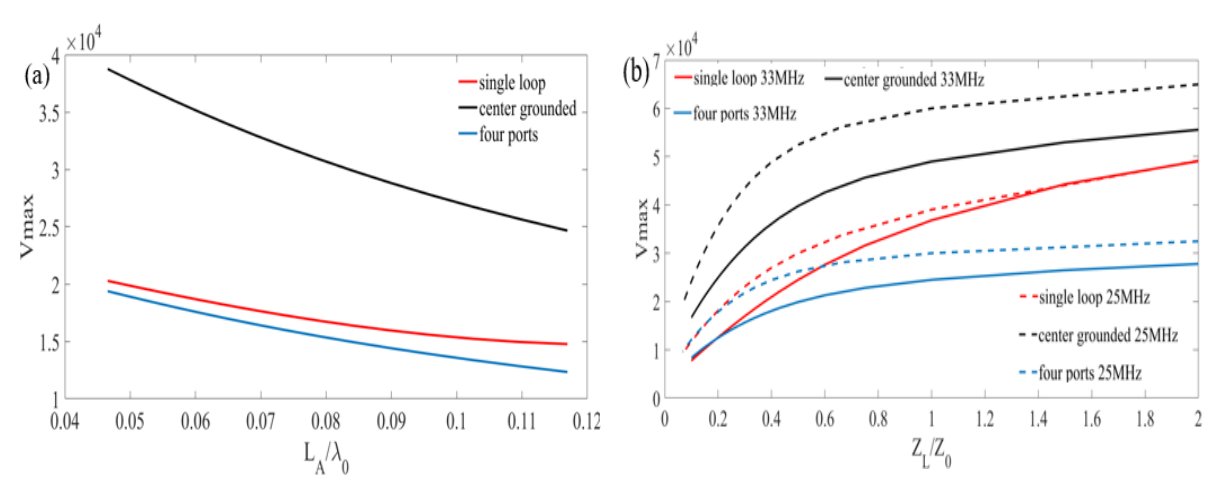


FIG 10. Comparison of  $V_{max}$  among three antenna configurations. (a)  $V_{max}$  VS the normalized electrical length,  $L_A/\lambda_0$ ; (b)  $V_{max}$  VS the normalized antenna load impedance,  $Z_L/Z_0$ .

Resonant Magnetic Perturbation (RMP) coils. Although the radial size of the RMP coil is going to be reduced from 8cm to 5cm to accommodate the antenna, it still put space constraints at the back of the antenna. Finally, the available radial space for the antenna installation is 9cm in the middle plan and 15cm in the poloidal extremities, as it is shown in FIG 11.

Given the present constraints, to fit the antenna into such a narrow space, two strategies are taken, 1. Put the short circuit at top and bottom so that the radial space is largest where the current is maximum. Part of the antenna backplate has to protrude towards the plasma in order to go over the RMP coils, as shown in Fig. 10 (a). 2. Remove the detour structure which connects the coaxial inner conductor and the strap, as shown in FIG 12 (c). The detour structure can increase the length of straps while introduce capacitance to reduce the strap inductance, and thus it

is frequently used in the present-day ICRF antenna. 3. Remove the antenna side limiter. All the antenna sides will be protected by the first wall blocks. The antenna box itself is supported by 8 stainless steel blocks already welded at the vacuum vessel wall, i.e., the green blocks shown in FIG 12(b).

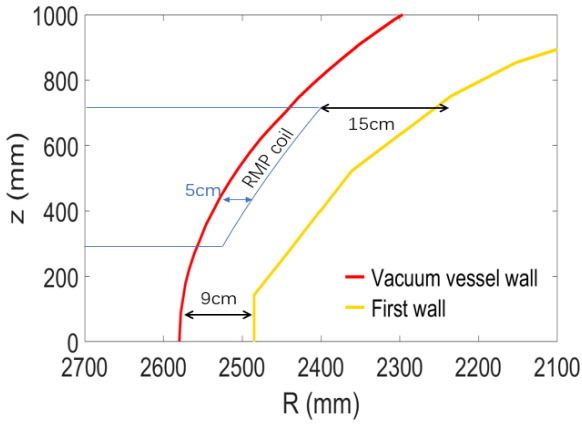


FIG 11. Space available for antenna installation inside the HL-3 vacuum vessel. The abscissa R represents the radial position, whereas vertical coordinate Z indicates the poloidal position.

In case this antenna does not work well, a backup plan is to feed the antenna through the upper and lower ports, instead of the middle plane port. FIG 13 shows the locations and dimensions of the upper and lower ports. At those places, the available radial space is larger. The present antenna shown in FIG 12 will be split into two parts. Each part will be fed by transmission lines coming through 2 ports, as depicted by the blue rectangles in the right Fig. of FIG 13. An off-middle plane ICRF antenna has not been tested yet in any tokamak device, although there is some modelling suggesting it may lead to different power deposition profiles compared to the middle plane injection [9]. Off middle plane injection may be also useful for a compact fusion reactor in the future. So if this backup plan is executed, it may also benefit future machines.

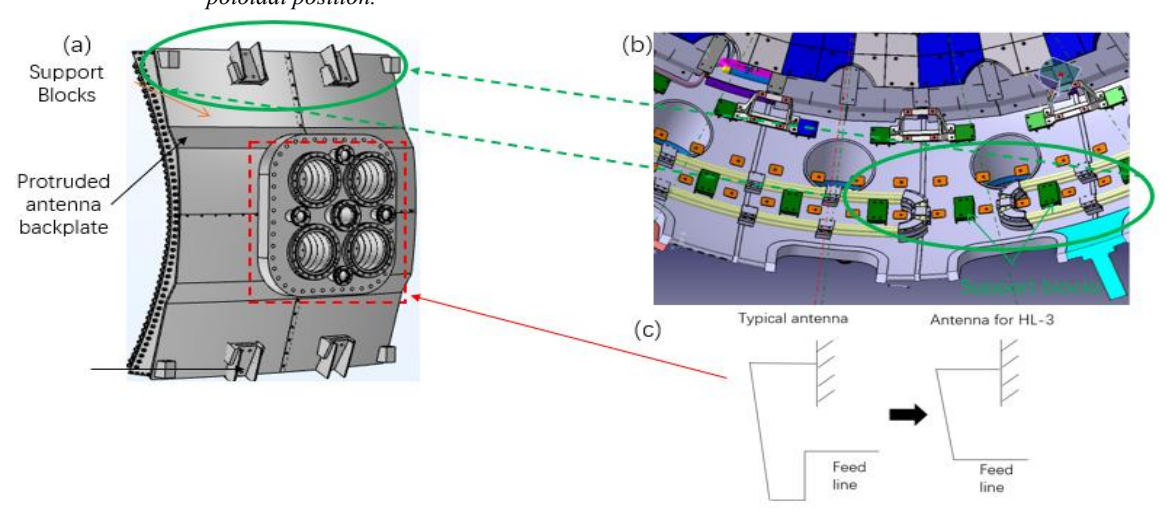


FIG 12. Left: Layout of ICRF antenna; Upper right: Display of the HL-3 vacuum vessel wall. RMP coils in yellow, support blocks in green. Lower right: Sketch of the feed line connection to strap.

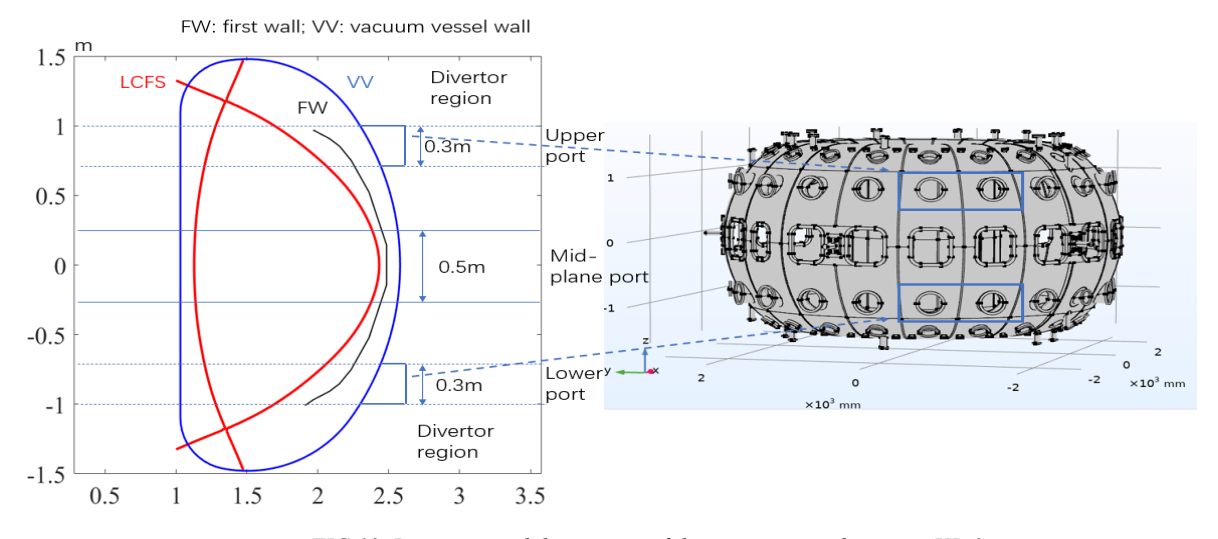


FIG 13. Locations and dimensions of the vacuum vessel ports in HL-3.

## 4.3 Thermal analysis

Due to the concerns of tritium contamination, water cooling is prohibited inside the vacuum vessel in HL-3 during D-T operation. It is thus important to evaluate the temperature rise of the antenna after 5s operation and assess the necessary time for its cooling down. A simplified antenna model which removes all the screws and holes is built in ANSYS. Simulation mainly considers the heat load contributed from the RF loss generated by skin current effects [10] and from the plasma radiation. The strap is made by Stainless steel 316L, with an electrical conductivity about  $2 \times 10^6 \text{S/m}$  at  $200^{\circ}\text{C}$ . Calculation shows the surface-averaged RF loss on the strap is about  $0.3 \text{MW/m}^2$  with the total input power of 3MW. While the Faraday screen is made by TZM alloy whose electrical conductivity is  $2 \times 10^7 \text{ S/m}$  at  $200^{\circ}\text{C}$ . The surface-averaged RF loss on the Faraday screen surface is only about  $0.06 \text{MW/m}^2$ . In terms of the plasma radiation, calculation shows the maximum heat load on the front face of the Faraday screen is about  $0.5 \text{MW/m}^2$ . In the ANSYS simulation, we assume the heat loads that are normally distributed on the strap surface is  $0.3 \text{MW/m}^2$ , and at the front face of the Faraday screen is  $0.6 \text{MW/m}^2$ . This is of course an exaggerated situation.

In the D-T campaign, hot wall operation is often used to reduce the tritium retention at wall. In HL-3, the vacuum vessel and first wall will be heated up to 150°C and 250°C respectively. In the following simulation, the antenna backplate is kept at a constant temperature of 200°C to mimic the hot wall operation. The initial temperature for the whole antenna is set as 200°C. During 5s full power injection, the temperature rise of each component is shown in FIG 14(a). The temperature at the Faraday screen, antenna box and strap are 473°C, 374°C and 324°C, respectively. FIG 15 also shows the temperature distribution on the antenna at t=5s, *i.e.*, after 5s full power ICRF operation in the hot wall mode. All of these are far less than the melting points of the 316L stainless steel (1400°C) and TZM (2623°C). Since there is no water cooling, the only cooling down mechanism is the heat transfer to the vacuum vessel. The time interval between two shots in HL-3 is 15mins typically. FIG 14(b) shows after 15mins cool down, the temperature at the Faraday screen, antenna box and strap reduce to 343°C, 331°C and 238°C, respectively. The antenna box and strap are bolted to the antenna box and the strap decreases faster than the Faraday screen. Not surprisingly, the temperature at the backplate rises a little bit, from 200°C to 240°C, after receiving the transferred heat from the other components.

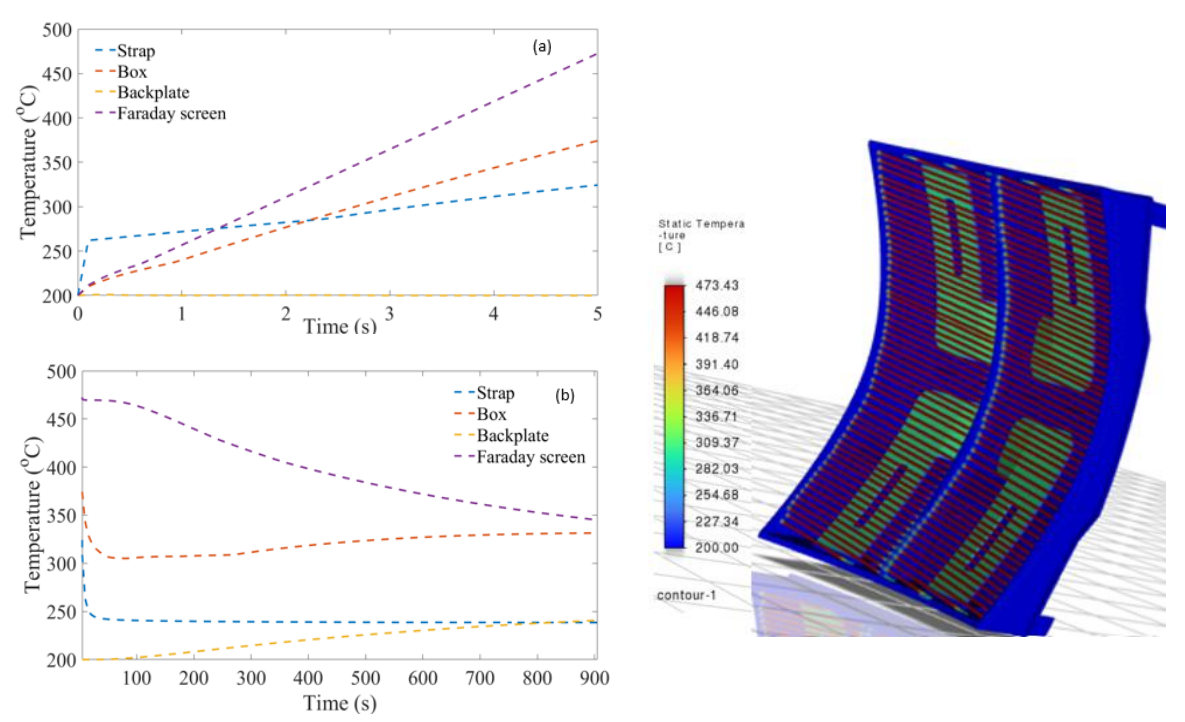


FIG 14. Temperature variations of each antenna component during heat up and cool down process in the hot-wall operation. Antenna injected power P=3MW.

FIG 15. Temperature distribution at antenna at t=5s with 3MW full power, hot wall operation, initial temperature=  $200 \, ^{\circ}\text{C}$ .

During the normal operation, the antenna backplate is attached to the vacuum vessel wall. In the ANSYS simulation, it is kept at a constant temperature of 25°C. The temperature rises of each antenna component are calculated under 3MW injected power, starting from room temperature, *i.e.*, 25°C at t=0s, up to 5s. Note 5s is

# [Right hand page running head is the paper number in Times New Roman 8 point bold capitals, centred]

already the maximum duration of the antenna operation. Most often, the antenna will operate about only 2-3s in most of the discharges. The temperature at the Faraday screen rises the quickest, up to 298°C at t=5s, while the temperature at the antenna box and strap are 199°C and 149°C, respectively. We further calculated the decrease of the antenna temperature after 900s. After 15mins, the Faraday screen, strap and antenna box are cooled to 168°C, 63°C and 156°C, respectively. As a comparison, the temperature at the backplate rises from 25°C to 65°C.

After the mechanical design, the antenna model is finally implemented in COMSOL to conduct the full wave simulation, as it was done previously for WEST [11]. It is checked that |E| is no more than  $2 \times 10^6$  V/m with the maximum injected power, P=3MW. Aside from the antenna design, antenna diagnostics are also essential to improve the power coupling and monitoring the antenna status during its operation. Each antenna in HL-3 will equip a middle plane gas puffing, a reflectometry, a couple of thermocouples and multiple kinds of probes, *i.e.*, the B-dot probe, phasing probe, voltage probe and Langmuir probe. The antenna will be installed in HL-3 around Sep. 2026 after being commissioned in a dedicated vacuum tank. The experiment test inside HL-3 is presently scheduled in 2027.

## 5. CONCLUSION

A new 6MW ICRF system is under construction at SWIP for HL-3 and it is foreseen to be complete in Sep. 2026. The frequency band is 25-50MHz, with the main operation frequency 33MHz for the Deuterium plasma and 25MHz for the Deuterium-Tritium plasma. Four transmission lines consists of 3dB combiner and decoupler, matching unit, antenna decoupler, T connector, double vacuum windows are designed. Simulation confirmed that with current matching unit set up, all the load impedances of our interest should have been covered. Two 2-strap antennas, with  $k_{l}$  ~6.5 m<sup>-1</sup>, fed by 4 ports, are designed. Antenna radial depth is constrained to be 9cm at middle plane and 15cm at the poloidal ends. Due to the constraint of radial space, the frequently used detour structure has to be removed. Thermal analysis has been done by ANSYS, while the electric analysis is done by full wave COMSOL model. It is concluded that under the extreme case (0.6MW/m² heat load normally distributed on the Faraday screen front surface, 0.3MW/m<sup>2</sup> normally distributed on the strap surface, antenna operates for 5s), the Faraday screen, antenna box and strap will be heated up to 298°C (473°C), 199°C (374°C) and 149°C (324°C) under the normal (hot-wall) operation, which is far less than the melting temperatures of the corresponding materials. So it is possible to operate the antenna without water cooling. However, antenna temperature must be monitored carefully to see whether it is sufficiently cooled down during the pulse gap. Further mechanical analysis to evaluate the Lorentz force acting on the antenna components during the major disruption or the vertical displacement event is undergoing and will be presented in the upcoming full-length paper.

# **ACKNOWLEDGEMENTS**

The authors would like to thank emeritus Prof. Jean-Marie Noterdaeme and Dr. Jean-Michel Bernard from CEA/IRFM for many useful discussions. This work is supported by National Magnetic Confinement Fusion Science program of China under the contract number 2022YFE03090002 and the National natural Science Foundation of China under grant agreements 12375212.

## REFERENCES

- [1] X. R. Duan et al, Nucl. Fusion **64**, 112021 (2024)
- [2] W. Zhong et al, this conference, OV /3-3 (2025)
- [3] L. F. Lu et al, Nucl. Fusion **63**, 066023 (2023)
- [4] L. Heikinheimo et al, Fus. Eng. & Des. 55, 419 (2001)
- [5] L. N. Liu et al, Nucl. Fusion **64**, 066025 (2024)
- [6] L. F. Lu et al, Nucl. Fusion 64, 126013 (2024)
- [7] V. Bobkov et al, Nucl. Mat. Energy 41, 101742 (2024)
- [8] R. Diab et al, Nucl. Fusion **65**, 076038 (2025)
- [9] Y. Lin, J. C. Wright and S. J. Wukitch, J. Plasma Phys. **86**, 865860506 (2020)
- [10] Q. C. Liang et al, Nucl. Eng. Tech. 55, 2621 (2023)
- [11] W. Tierens et al, Nucl. Fusion **64**, 126039 (2024)